



High-performance displacement by microgel-in-oil suspension in heterogeneous porous media: Microscale visualization and quantification

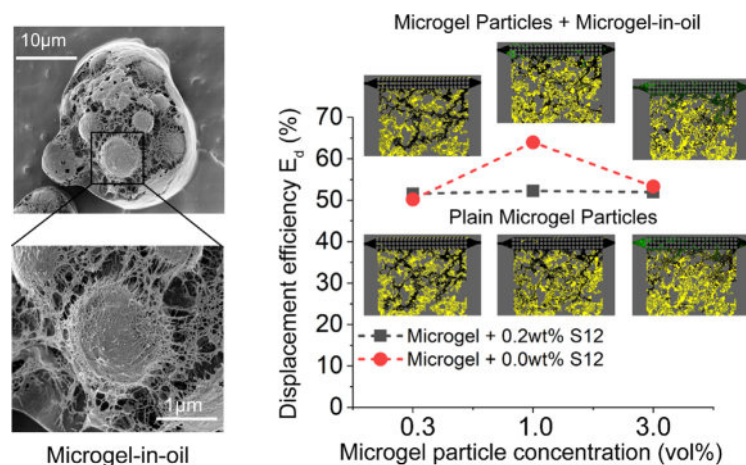
Wenhai Lei^a, Xukang Lu^a, Tianjiang Wu^b, Haien Yang^b, Moran Wang^{a,*}

^a Department of Engineering Mechanics, Tsinghua University, Beijing 100084, China

^b Changqing Oilfield, PetroChina, Xi'an, Shaanxi 710018, China



GRAPHICAL ABSTRACT



ARTICLE INFO

Article history:

Received 2 May 2022

Revised 15 June 2022

Accepted 19 July 2022

Available online 21 July 2022

Keywords:

Microgel-in-oil

Microgel particle suspension

Microfluidics

Multiphase flow

Displacement mechanism

ABSTRACT

Hypothesis: Preferential flow in porous media is commonly encountered and decreases the multiphase displacement efficiency. Here, we synthesized microgel-in-oil in suspension and demonstrated that microgel-in-oil as a novel additive could present self-adaptive transport behavior and introduce a novel multiphase displacement mode for improving displacement efficiency in heterogeneous porous media.

Experiments: We investigated the microgel-in-oil formation process and characterized their morphology with fluorescence microscopy and Cryo-SEM. The suspension displacement performance in heterogeneous porous media was evaluated using a microfluidic chip containing a preferential flow pathway (PFP) and a parallel matrix region. The displacement results of microgel-in-oil were compared to plain microgel particles and analyzed from pore-scale particle transport behavior to macroscopic multiphase flow patterns.

Findings: The results show that suspension with moderate microgel-in-oil yields the optimal displacement efficiency. Fewer microgel-in-oil cannot alter the flow direction, while too many microgel-in-oil would block the PFP region. The topological analysis identified that suspensions with moderate microgel-in-oil content could achieve the strongest sweeping and carrying abilities that contribute to the highest displacement efficiency. The synergistic transport of microgel-in-oil and plain microgel

* Corresponding author.

E-mail address: mrwang@tsinghua.edu.cn (M. Wang).

particles would result in local pressure fluctuations to divert displacing fluid from PFP into the matrix region, which explains the above flow behavior.

© 2022 Elsevier Inc. All rights reserved.

1. Introduction

Multiphase displacement in porous media has drawn extensive research attention due to its importance in various natural and industrial processes, such as hydrocarbon recovery [1], contaminated soil and groundwater remediation [2], geological carbon sequestration [3], solar water splitting [4], and biomaterials fabrication in microfluidic chips [5]. In these porous systems, the heterogeneity of hydraulic property widely exists, which induces the displacing fluid preferentially flowing through pathways with the lowest resistance rather than through other matrix parts [6–8]. When the preferential flow bypasses the matrix region, transferring the displacing fluid into the matrix area is a significant technical challenge as there is nearly no net fluid flow [9–11]. Dissolving high molecular weight polymers in water has been successfully implemented to suppress preferential flow through increasing the displacing fluid viscosity [12,13]. However, merely increasing the viscosity may not further improve the efficiency of multiphase displacement [14–16]. More importantly, injection capacity reduction, shear degradation, and dilution effect lead to unguaranteed application results [17–19].

To overcome the above drawbacks, microgel particle suspensions have been developed as attractive agents with several remarkable properties, such as easy preparation, good controllability, environmental friendliness, and adaptation to complex environments [20–23]. Microgel particles are stable, micron-scale, water-soluble, and non-toxic polymer particles [24,25]. Various microgel particles have been applied in the engineering applications, including preformed particle gel (PPG) [26], soft microgel (SMG) [27], dispersed particle gel (DPG) [28], colloidal dispersion gel (CDG) [29] and polymer microspheres (PMs) [30]. These suspensions have the polymer/colloid duality, showing the viscoelasticity of complex fluid and the transport behavior of particles [31,32]. Compared with water-solute polymers, microgel particle suspensions have better injectability and a more substantial impact on displacement efficiency [33,34]. The excellent capability of microgel particle suspensions is commonly claimed to have advantages in blocking the high-permeability pathways and then diverting the displacing fluid into low-permeability layers [18,26]. Extensive studies have been conducted to elucidate this diversion effect by the size matching rule between the particles and pores. Bai, et al. [35] reported sharp pressure pulses at the clogging-remigration positions of microgel particles and determined the optimal particle diameter as 2–4 times the pore size through microfluidic experiments. Lin, et al. [33] found that the optimal size matching relation was 0.33–0.50 via the nuclear pore membrane filtration experiments. Dai, et al. [28] presented the optimal size matching factor ranging from 0.21 to 0.29 depending on the injection pressure and the plugging rate via the coreflooding experiments. Zhao, et al. [36] also found that smaller particles containing higher elastic modulus can enhance plugging capability during the coreflooding experiments. The abovementioned results with a wide size matching range indicated that size matching is not the only mechanism for improving displacement efficiency by the microgel particle suspension. A more fundamental understanding of displacement mechanisms by microgel particle suspension may require pore-scale visualization and quantification of real-time suspension flow in porous media, which has not been fully explored yet.

Microfluidics has provided a platform to conveniently visualize multiphase displacement and particle behavior in micron-scale porous structures [37–39]. In the past decades, breakthroughs have been made in the enhancement of structure realism within microfluidic chips, such as reservoir-on-a-chip [40], soil-on-a-chip [41], coreflood-on-a-chip [42], steam-on-a-chip [43], etc. On-chip porous media facilitate our focus on the statistical results of displacement at the macroscopic scale and simultaneously unique flow behavior at the pore scale [40,44]. However, the heterogeneous porous structure in nature and engineering brings a great challenge to microfluidic research on the impact of microgel particle suspension on multiphase displacement. On the one hand, although various complex fluid flooding mechanisms have been explored in previous pore-scale studies, directly translating those results to the impact of microgel particle suspension on the displacement efficiency may not be feasible because of the loss of the statistical characteristics of heterogeneous porous structures. Wan, et al. [45] first investigated directly the single-phase flow velocity profile in the fracture-matrix porous media based on hand-drawing patterns in a glass micromodel. The multiphase displacement process in the dual-permeability microfluidic chip with vertical post arrangements has also been addressed. The preferential flow suppression effect of foam [46,47] and microgel particle suspensions [8,31,34] have been elucidated. To further purify the emulsion flow mechanism, Xu, et al. [48] designed the channel-type micromodel with multiple parallel high- and low-permeability pathways and showed the emulsion-blockage performance on sweep-efficiency improvement. These designed structures appear heterogeneous at the pore level or random at the macroscopic view but do not satisfy structure representations in nature and engineering. On the other hand, the microgel particle suspension may exhibit unique behavior in the porous media due to the complex flow conditions and porous geometrical confinement. The in-situ properties of the microgel particle suspension in porous media may be different from bulk properties, which is responsible for the multiphase displacement consequences [31,49]. In order to synthesize ideal displacing fluid, optimize the displacement operations and thus improve displacement efficiency, it is crucial to visualize and quantify the real-time performance of microgel particle suspensions in representative heterogeneous porous structures.

In this work, inspired by the emulsion of microgel particles as high-performance bio-lubrication additives in food science and biomedicine, where several oil droplets are trapped within a biopolymer hydrogel particle [50–52], we firstly discovered and synthesized the new compound particles in the microgel particle suspension where several microgel particles are trapped within the oleic droplet and elucidated their high performance in improving the displacement efficiency in the heterogeneous porous media. When the stock microgel particle suspension is prepared by the inverse suspension polymerization method and diluted in water to a specified concentration, most microgel particles will disperse from the droplet of the stock suspension. Some microgel particles may still be trapped in oil droplets in the suspension, called microgel-in-oil. With the visualization of multiphase displacement on microfluidic chips with heterogeneous porous structures, we evaluated the displacement performance of microgel particle suspensions in the presence of microgel-in-oil, in contrast to plain microgel particles. We observed different microgel-in-oil transport

modes by varying the particle concentrations and quantified the corresponding displacement efficiency. Our visualization system permits real-time imaging of the displacement processes from a local view to the scale of the entire microchip. The topology analysis of displacement pattern evolution enables us to evaluate displacing fluid's sweeping and carrying ability. Combining injection pressure, oil ganglion topology, and displacement efficiency curves during the flooding process, the synergistic transport of microgel-in-oil and plain microgel particles can explain the multiphase displacement mechanism. This discovery illustrates the impact of microgel-in-oil on the multiphase displacement process in heterogeneous porous media, which may lead to new techniques for high-performance displacement in many applications, such as enhanced oil recovery, soil remediation, and geological carbon sequestration.

2. Materials and methods

2.1. Microgel particle synthesis

The stock microgel particle suspension is synthesized by the inverse suspension polymerization method. In the synthesis process, the aqueous monomer solution is divided into several reactive microdomains in the oleic phase by a dispersion stabilizer to produce microgel particles. The chemical reagents for microgel particle synthesis include acrylamide (25%, purity above 98.5%), solvent 1 (30%, mineral oil), deionized water (20%), dispersion stabilizer (15%, Span 60 & Tween 60), water-soluble anionic monomer (5%, acrylic acid & sodium acrylate), third monomer (3%, acrylate), and solvent 2 (2%, xylenes). They are all purchased from Shanghai Macklin Biochemical Co., Ltd (China) without further purification. To observe the microgel particles more clearly, we added the fluorescence on the surfaces of all microgel particles in the laboratory of Technical Institute of Physics and Chemistry, Chinese Academy of Sciences.

2.2. Preparation of microgel particle suspensions

Firstly, we mixed the stock microgel particle suspension and mineral oil containing 15% Span 60 as a volume ratio of 2:1 to increase the oil content in the suspension. Then we prepared the microgel particle suspension with the required concentration (0.3–3.0 vol.%) by diluting the stock microgel particle suspension in deionized water, which was stirred at 800 r/min for 3 min. For comparison, 0.2 wt.% sulfobetaine 12 (S12, Macklin) was dissolved in the above microgel particle suspensions to decompose the microgel-in-oil in the suspension during the diluting process. Finally, stand for ten minutes, remove the upper oil layer caused by demulsification and take off the uniform suspension in the lower layer to conduct the experiments.

2.3. Characterization methods

The cryo-scanning electron microscope (Cryo-SEM, Helios NanoLab G3UC, USA), equipped with Quorum PP3010T cryo-system, was used to observe the in-situ morphology of the microgel particles in the suspension. In the experiments, the structure of microgel particles in the stock suspension as the original states were compared with that in the diluted aqueous suspension.

The distribution of microgel particles in the suspension was observed via a fluorescence microscope (Nikon, SMZ18, Japan). The bandpass wavelengths of the excitation filter ($\lambda_{\text{ex}} = 460\text{--}500$ nm) and receiving filter ($\lambda_{\text{em}} = 510$ nm) match the excitation and emission wavelengths of the fluorescent microgel particles. 100 ppm Nile red dyed the oleic phase (decane), and their fluores-

cent peak excitation wavelength λ_{ex} is 493 nm, and emission wavelengths λ_{em} is 510 nm. To observe the suspension formation process, we dropped the new diluted suspension (after rapid stirring 30 s) on a clean glass slide, put another glass slide on it, and immediately observed it under the fluorescence microscope.

The particle size distributions of microgel particle suspensions were measured via a Malvern Mastersizer 3000E Hydro (Malvern Instruments, Worcestershire, U.K.) using refractive indices of microgel particles and the aqueous phase of 1.50 and 1.33, respectively.

Rheological characterization was performed using a rheometer (Haake Mars III, Thermo Fisher Scientific, USA) equipped with a stainless steel upper cone plate as a clamping fixture (diameter 60.006 mm, cone angle 0.989°, model C60/1° TiL). Viscosity curves were obtained from the different samples under state shearing modes as a function of shear rate, ranging from 0.01 to 10 s^{-1} at 20 °C.

Wettability characterization was conducted by Drop Shape Analyzer (DSA25, Krüss, Germany) using Young-Laplace fitting method. Before measuring contact angle, all substrate was ultrasonically cleaned with acetone, absolute ethanol, and deionized water for ten minutes sequentially, then dried and soaked in decane for 24 h. The system wettability was characterized by placing a small drop of injection fluid on the substrate submerged in a decane-filled reservoir. Contact angles of different injection fluids with the immersion time were measured until they were relatively stable without change qualitatively with time. Contact angles measured here are used to characterize the intrinsic contact angle of microfluidic chips.

2.4. Microfluidic chip design and fabrication

The preferential flow is inevitable in engineering applications due to the geometrical heterogeneity of porous solids, interfacial instability, or asymmetrical injection methods, as shown in Fig. 1a. To mimic preferential flow conditions, we designed a microchip with a heterogeneous porous structure leading to a controllable and repeatable PFP, as shown in Fig. 1b. The microchip structure is divided into the PFP and matrix regions. Corresponding pore size distributions were obtained from a 3D microcomputed tomography (μ -CT) scanning image of a natural rock sample in the Changqing oil field, China. Argon Ion Milled-Scanning Electron Microscopy (SEM) presented the pore morphology. The pore structure in the PFP zone is large, uniform, and concentrated, but that in the matrix zone is small, complex, and scattered, as shown in Fig. 1c. Based on these structure characteristics, the matrix zone was first designed using the regeneration method proposed by Lei, et al. [34], reflecting the statistical information of natural rocks. The second step of creating a heterogeneous porous structure entails the addition of a higher-permeability zone parallels to the matrix zone to establish a PFP actively. A similar design method to that of the matrix zone could undoubtedly be adopted to produce this PFP zone, yet to enhance the repeatability of the experiments, we chose particle packing structures and applied them in the PFP region in this work. The solid porous structures and their pore size distributions are shown in Fig. 1d. The porosity of the PFP region is the same as that of the matrix region, but the permeability ratio is around 16:1, which has been calculated by the 3D single-phase lattice Boltzmann method (LBM) [53]. The pore volumes (PVs) of the PFP and matrix region are 0.15 μL and 0.84 μL , respectively. The 3D hydraulic diameter of pores ranges from 1.5 μm to 70 μm (Fig. 1d).

Considering the designed small and dense pore geometries, we fabricated the microchips with the silicon wafer, which has the advantages of high etching precision and a large aspect ratio compared to wet-etched glass [39]. After the design pat-

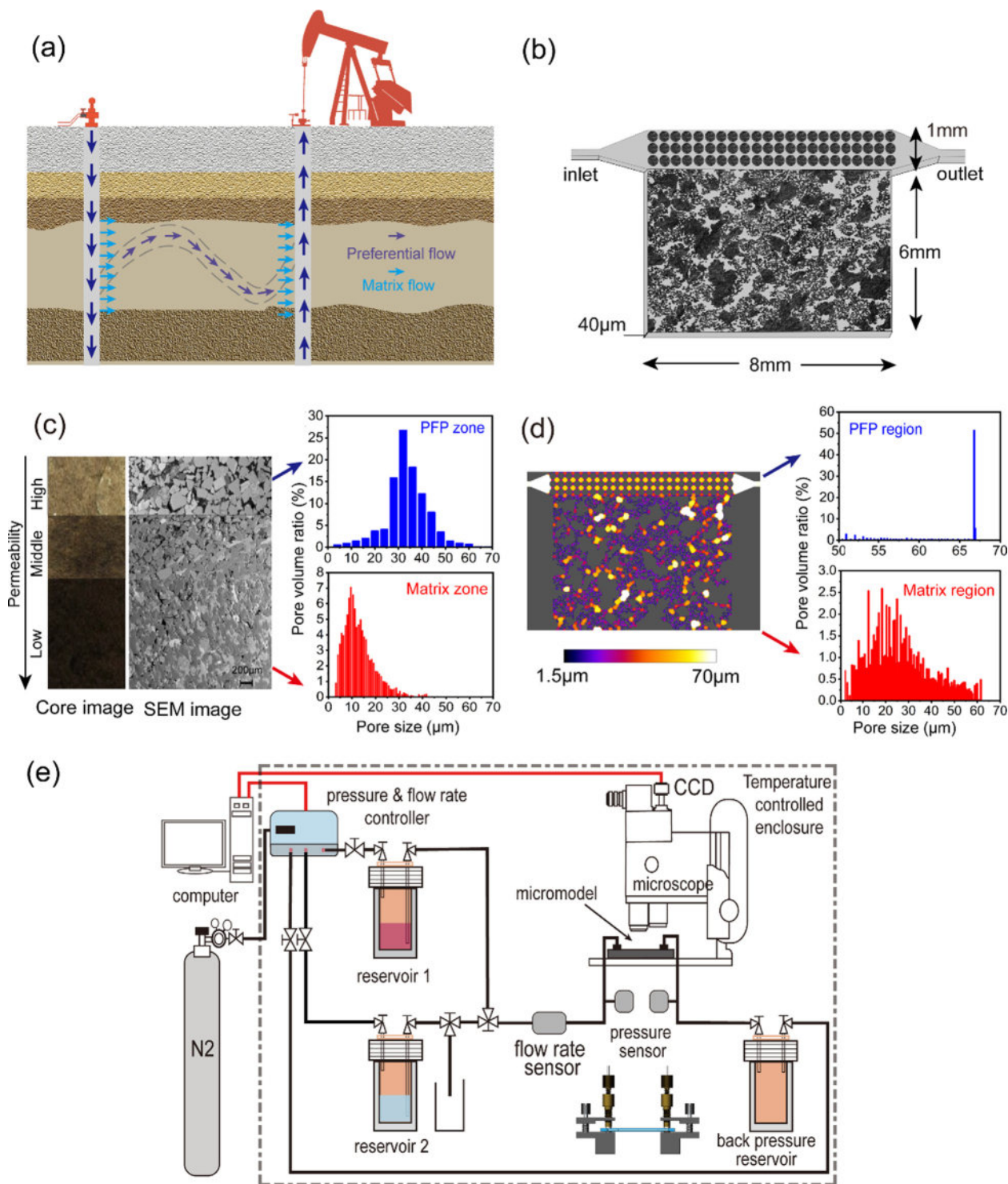


Fig. 1. Microchip designs and corresponding experimental setup. (a) Schematic diagram of preferential flow in geological engineering. (b) Macroscopic geometry information of the microchip. (c) Sandstone plugs drilled from inspection wells in the Changqing Oilfield, China, with different crude oil saturations (the strongly swept region is relatively white with a low crude oil saturation; conversely, the region is black due to a high crude oil saturation). The corresponding pore structures are characterized based on 2D scanning electron microscopy (SEM) and 3D microcomputed tomography (μ -CT) image stacks. (d) Hydraulic diameter map of the microchip and 3D pore size distributions of the PFP and matrix regions. (e) Schematic diagram of the experimental setup (black lines are fluid tubes, and the red lines are electric signal transmission lines).

terns were imported into AutoCAD using LISP (List Precession Language) [40], the porous structures were made from a silicon wafer using micro-fabrication techniques [54], including standard photolithography and inductively coupled plasma-deep reactive ion etching (ICP-DRIE). The pattern silicon wafer was then anodically bonded to the Pyrex glass wafer (Schott,

German). The upstream and downstream of those glass wafers were drilled with 2 mm diameter holes for the inlet and outlet of the microchip. The microchips were washed with dilute hydrochloric acid (2–3 vol.%), dichlorodimethylsilane at 1 mL/hour, and put in the fume hood for 24 h to keep the neutral-wet condition.

2.5. Experimental setup and operation

The cleaned microchip was assembled by a custom-designed fixture and observed under the fluorescence microscope. The experimental setup (Fig. 1e) consists of the injection system, a fluorescence microscope, a computer, and a microfluidic chip. The injection system includes a microfluidic pressure controller (Fluigent, MFCS-8C), a flow rate sensor (Fluigent, FRP), a pressure transducer (Validyne, P61), and three reservoirs. After treating the microchip in a vacuum for 12 h, the fluorescent dyed oil (100 ppm Nile red in decane) in Reservoir 1 was injected until all pores of the microchip were filled. Then, the switch changed to Reservoir 2 (the displacing fluid) to start the displacement experiments. Reservoir 3 was used as a waste liquid pool and back-pressure controller (1 psi gas pressure). The experiments were performed at a constant flow rate (1 $\mu\text{L}/\text{min}$). The characteristic capillary number is about 2.6×10^{-6} – 1.3×10^{-5} , corresponding to previous pore-scale studies [10,55] and engineering conditions [1,56]. The total injection time for each experiment was about 5 h to ensure a final changeless phase saturation (an incremental recovery lower than 0.1% per 1 PV of injection).

2.6. Image processing and data analysis

The displacement processes have been quantified by image processing and data analysis. In the microfluidic experiments, we used a spatial resolution of 1.92 μm and a time resolution of 1 s to meet the requirement of quasi-static experiments and analyze phenomena from micron-scale to centimeter-scale. The Image Processing Toolbox of MATLAB was applied with a self-developed program to analyze the various phenomena. First, the experimental images were converted into a binary form with displaced fluid in white and displacing fluid in black. Then, the white and black pixel ratio was counted to calculate displacement efficiency. Finally, the evolution of ganglion number and volume fraction of larger displaced fluid clusters were identified to evaluate displacement performance quantitatively.

3. Results and discussion

3.1. Morphological characterization

The formation process of microgel-in-oil in the suspension is illustrated in Fig. 2a. Microgel particles were initially prepared in the oleic phase and then diluted in the aqueous phase. Cryo-SEM of the stock microgel particle suspension and the diluted microgel particle suspension at various magnifications are presented in Fig. 2b. The microgel particles are well-dispersed in the stock microgel particle suspension, and their particle size is relatively uniform. However, in the diluted microgel particle suspension, microgel-in-oil appears aggregated with several times a single microgel particle diameter. Under higher magnification, the internal structure of microgel particles can be observed, where a porous interconnected network of polymer chains forms the spherical particle (Fig. 2b). In our experiments, the particle swelling in water may increase the particle size a little bit during the flow and displacement, but the particle size even after swelling is still much smaller than the pore size.

Fluorescence microscope observations on the microgel-in-oil formation process are shown in Fig. 2c. Most microgel particles (green color) were initially entrapped in oil droplets (yellow color), then particles were released from the oil droplets rapidly and soon reached stability after 200 s. Some particles were still trapped in oil droplets during the dilution process. Fig. 2d presents the fluorescence microscope micrographs of the microgel particle suspension

with 1 vol.% particle concentration in the absence and presence of 2 wt.% surfactants (Sulfobetaine 12, S12). To show the phase state of the microgel particle suspension more clearly, we did not dye the oil phase of the stock solution. It is evident that dissolving surfactant-S12 in the suspension makes many microgel-in-oil decompose into well-dispersed particles, and microgel-in-oil content is significantly reduced.

Some experimental and theoretical studies showed that microgels could reduce interfacial tension and stabilize emulsions due to particle deformation [57–59]. Some recent theoretical studies have also proved that oil adsorption by the microgel can create a polymer shell around the absorbed oil droplet, thus practically all oil components will be concentrated within the microgels and remain stable toward aggregation [60,61]. These studies may explain why the microgel-in-oil can maintain stability, but the microscopic formation mechanism of the microgel-in-oil is still unclear. More microscopic mechanisms and accurate control of the microgel-in-oil formation need to be considered in the future work.

3.2. Particle size distribution (PSD), rheology, and wettability characterization

The PSDs of the diluted microgel particle suspensions with different particle and surfactant-S12 concentrations were examined (Fig. 3a–c). The PSDs were monomodal and similar at low particle concentration (0.3 vol.%) with a mean particle size $d = 4.58$ – 7.64 μm (Fig. 3a). When the microgel particle concentration increased to the intermediate concentration (1.0 vol.%), the addition of surfactant-S12 (0–0.2 wt.%) significantly affected the PSD (Fig. 3b). Microgel particles without surfactant displayed bimodal particle size distribution. Microgel-in-oil was generated with a mean particle size $d = 127$ – 144 μm as several microgel particles were aggregated and encapsulated in oil droplets. The addition of surfactant-S12 could decompose the microgel-in-oil, and the PSDs finally shifted to monomodal type with only small plain microgel particles when the surfactant-S12 concentration reached 0.2 wt.% (Fig. 3b). However, the PSDs at high particle concentration (3.0 vol.%) maintained the bimodal type, and the microgel-in-oil content was comparable to the small plain microgel particles (Fig. 3c). The sizes of well-dispersed microgel particles are much smaller than the hydrodynamic diameter of the microchannel in the PFP region (less than 1/10). However, the sizes of microgel-in-oil are comparable with the pore size in the PFP region.

The viscosities of microgel particle suspensions with different surfactant-S12 concentrations (0–0.2 wt.%) were measured to present how the particle concentration and the microgel-in-oil content affect the suspension rheology (Fig. 3d–f). The viscosities of microgel particle suspensions under all conditions decreased with increasing shear rate, i.e., suspensions exhibited typical shear-thinning properties. Viscosity measurements of microgel particle suspensions in the absence or presence of surfactant-S12 indicate that higher microgel-in-oil content contributes to higher viscosity.

Fig. 4 presents the different wettability of the aqueous fluid-decane-silicon systems. The aqueous fluid is microgel particle suspensions with different particle concentrations in the presence and absence of surfactant-S12, and water is used as a comparison. The wettability of all systems is between weakly water-wet and neutral conditions (contact angle ≈ 60 – 90°). A higher particle concentration will lead to a lower contact angle, and the presence of surfactant-S12 in the suspension can decrease the contact angle slightly.

3.3. Microgel particle suspension flooding

To emphasize the critical displacement effect of microgel-in-oil, we performed a series of displacement experiments on the

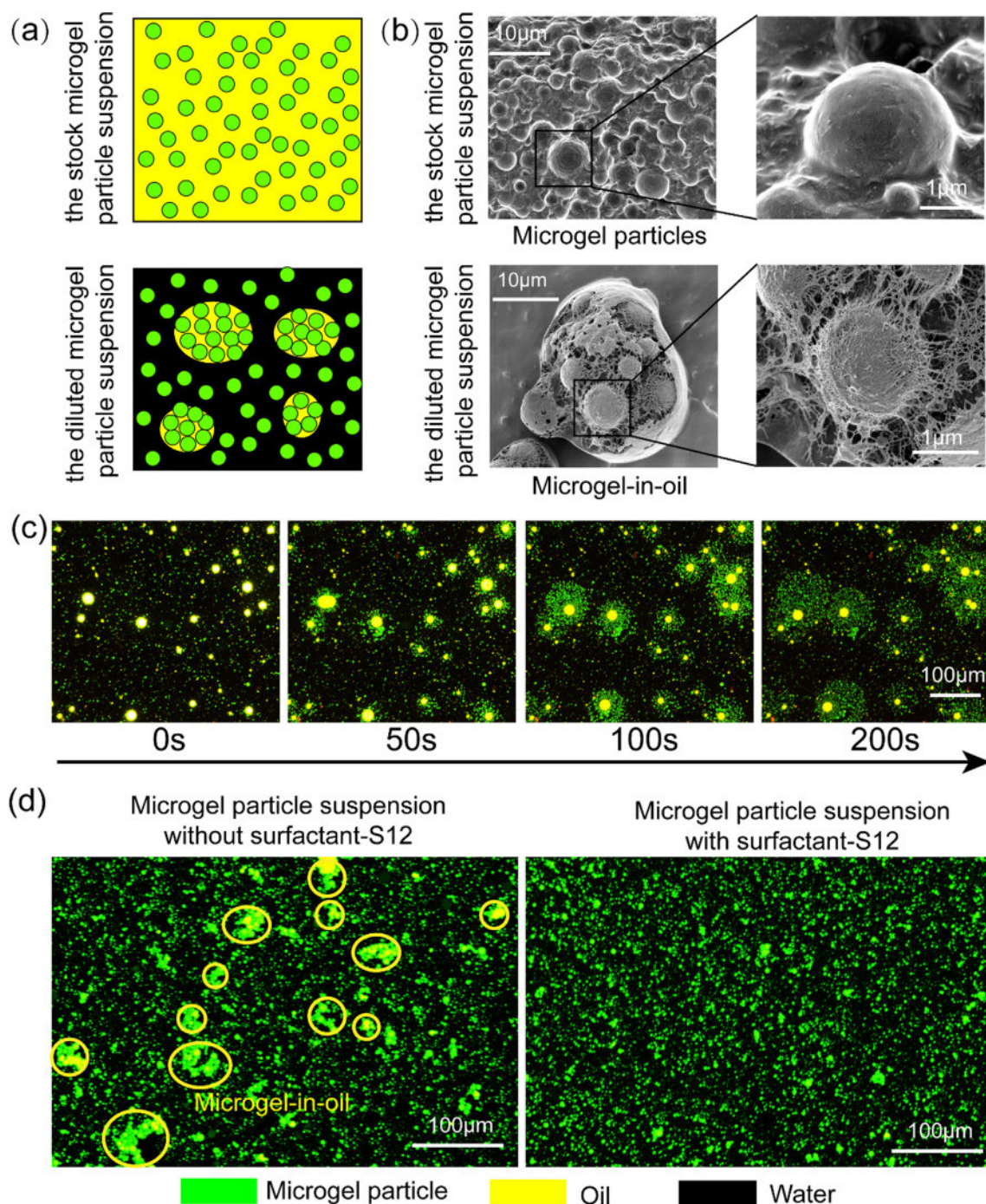


Fig. 2. (a) Schematic of microgel-in-oil formation by diluting the stock microgel particle suspension in water. (b) Cryo-SEM micrographs of the stock microgel particle suspension (up) and the diluted microgel particle suspension (down), showing the external structure (left) and local view of microgel particles (right), respectively. (c) The formation process of the microgel particle suspension. The stock microgel particle suspension in the oleic phase was dispersed in water, and the particles were released from the oil droplets within 200 s. (d) The fluorescence micrographs of microgel particle suspensions in the presence or absence of microgel-in-oil can be controlled by the surfactant-S12.

microfluidic chips with the heterogeneous porous structure. Fig. 5 presents the displacement patterns at the final stage. Here, the displacement processes of microgel particle suspensions with varying particle concentrations were visualized and quantified, and 0.2 wt. % surfactant-S12 was added to decrease the microgel-in-oil content in the suspensions as the comparison group (Fig. 3). At low particle concentration (0.3 vol.%), the content of microgel particles is too low to be observed directly in both cases with and without the surfactant-S12. The displacing flow patterns are relatively sim-

ple, mainly in the larger channels of the matrix area, as shown in Fig. 5 a,b. At high particle concentration (3.0 vol.%), the PFP region is blocked by microgel particles in both cases. The invading flow patterns are relatively complicated, but a small amount of displacing fluid can reach the deep matrix region with discontinuous flow channels, as shown in Fig. 5 e,f. It is difficult for fewer microgel-in-oil to alter flow direction in such a heterogeneous structure, while too many microgel-in-oil thoroughly blocking the PFP region limits the displacing fluid to flow into the deep matrix region. At interme-

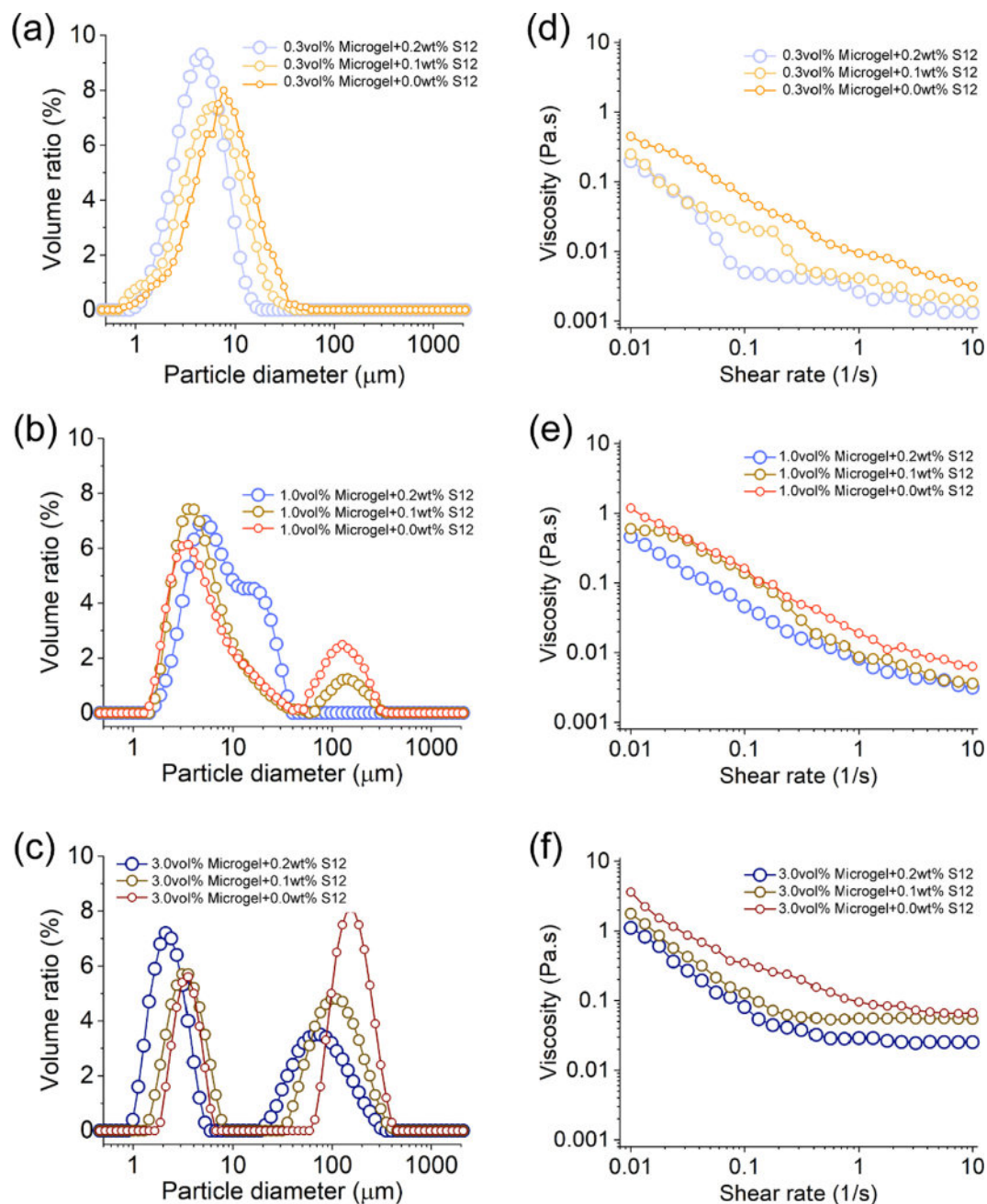


Fig. 3. Particle size distributions of microgel particle suspensions with (a) 0.3 vol.% (b) 1.0 vol.% and (c) 3.0 vol.% particle concentration with different surfactant-S12 concentration (0, 0.1, and 0.2 wt.%). Viscosity versus shear rate of microgel particle suspensions with (d) 0.3 vol.% (e) 1.0 vol.% and (f) 3.0 vol.% particle concentration with different surfactant-S12 concentration (0, 0.1, and 0.2 wt.%) at 20 °C.

diate particle concentration (1.0 vol.%), the suspension without surfactant-S12 has moderate microgel-in-oil content (Fig. 3b), which can temporarily block and transport through the PFP region to achieve the highest displacement efficiency, as shown in Fig. 5c. In contrast, the addition of surfactant-S12 decomposes microgel-in-oil such that microgel particles pass the PFP region directly, as shown in Fig. 5d. Although the presence of surfactant-S12 can slightly decrease the contact angle (Fig. 4), the wettability effect on displacement performance is nearly ignorable [55]. These displacement patterns present that microgel particle concentration and microgel-in-oil content largely influence displacement results.

Variations in displacing fluid saturation S_d versus time and displacement efficiency E_d for the displacement experiments with different particle concentrations in the absence or presence of

surfactant-S12 are calculated (Fig. 6). The waterflooding under the same condition is introduced for comparison. As expected, the displacement performance in the suspension system is much better than in waterflooding, as shown in Fig. 6d. Among all floods, microgel particle suspension at intermediate particle concentration (1.0 vol.%) in the absence of surfactant-S12 attain the highest displacing fluid saturation that effectively displaces oil from the matrix region (Fig. 5c and Fig. 6d). Fig. 6b presents that the moderate content of microgel-in-oil leads to a continuous incremental displacing fluid saturation and eventually reaches a high level.

These suspension systems have a similar displacement behavior at the breakthrough stage, as shown in Fig. 6e. It also demonstrates that the suspension rheology nearly does not affect displacing fluid saturation in such high flow heterogeneity conditions due to the

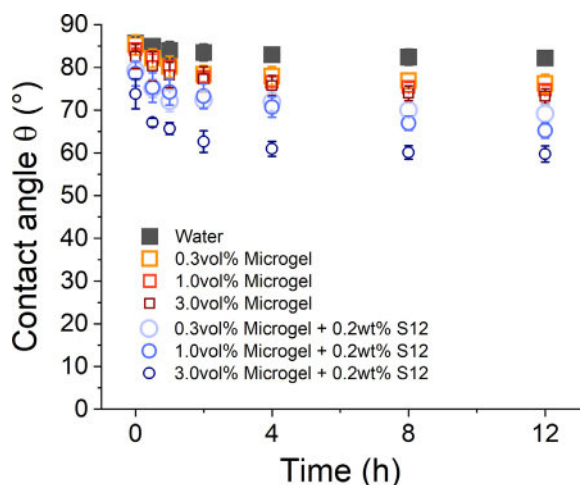


Fig. 4. Contact angle variation with time for suspension with different particle concentrations in the present and absence of surfactant-S12.

viscosity effect usually working before the breakthrough stage [31]. However, it is interesting that their displacement efficiency increases largely at the final stage, and 1.0 vol% microgel particle suspension in the absence of surfactant-S12 shows a more pronounced recovery behavior – 10.67 ~ 13.80% displacement efficiency higher than in other cases (Fig. 6f). These results indicate that the displacement in the matrix region continues for a long time after the breakthrough. The moderate content of microgel-in-oil significantly impacts the matrix flow pattern and eventually increases the displacement efficiency.

3.4. Statistical analysis of ganglion evolution

The topology of displaced fluid in the matrix region strongly controls the multiphase displacement consequences, which can be observed and statistically analyzed by ganglion evolution in our microfluidic experiments. We recognized each oil ganglion and quantified the flow patterns by two typical metrics during the displacement process: oil ganglion number and volume frac-

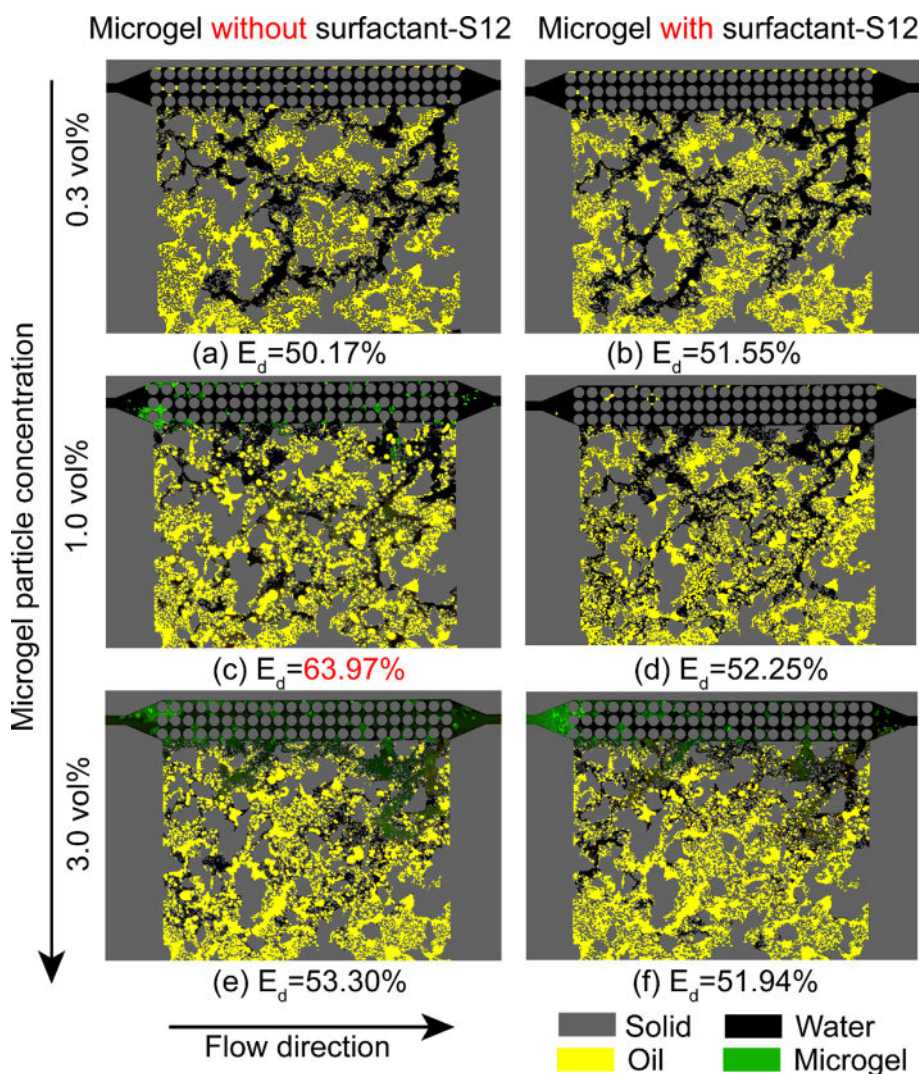


Fig. 5. Snapshots of the multiphase distribution in the porous media at the final stage. Microgel particle suspension flooding at (a, b) low particle concentration 0.3 vol.%, (c, d) intermediate particle concentration 1.0 vol.%, and (e, f) high particle concentration 3.0 vol.%. (a, c, e) The displacement results of microgel particle suspensions without surfactant-S12. (b, d, f) The displacement results of microgel particle suspensions with surfactant-S12.

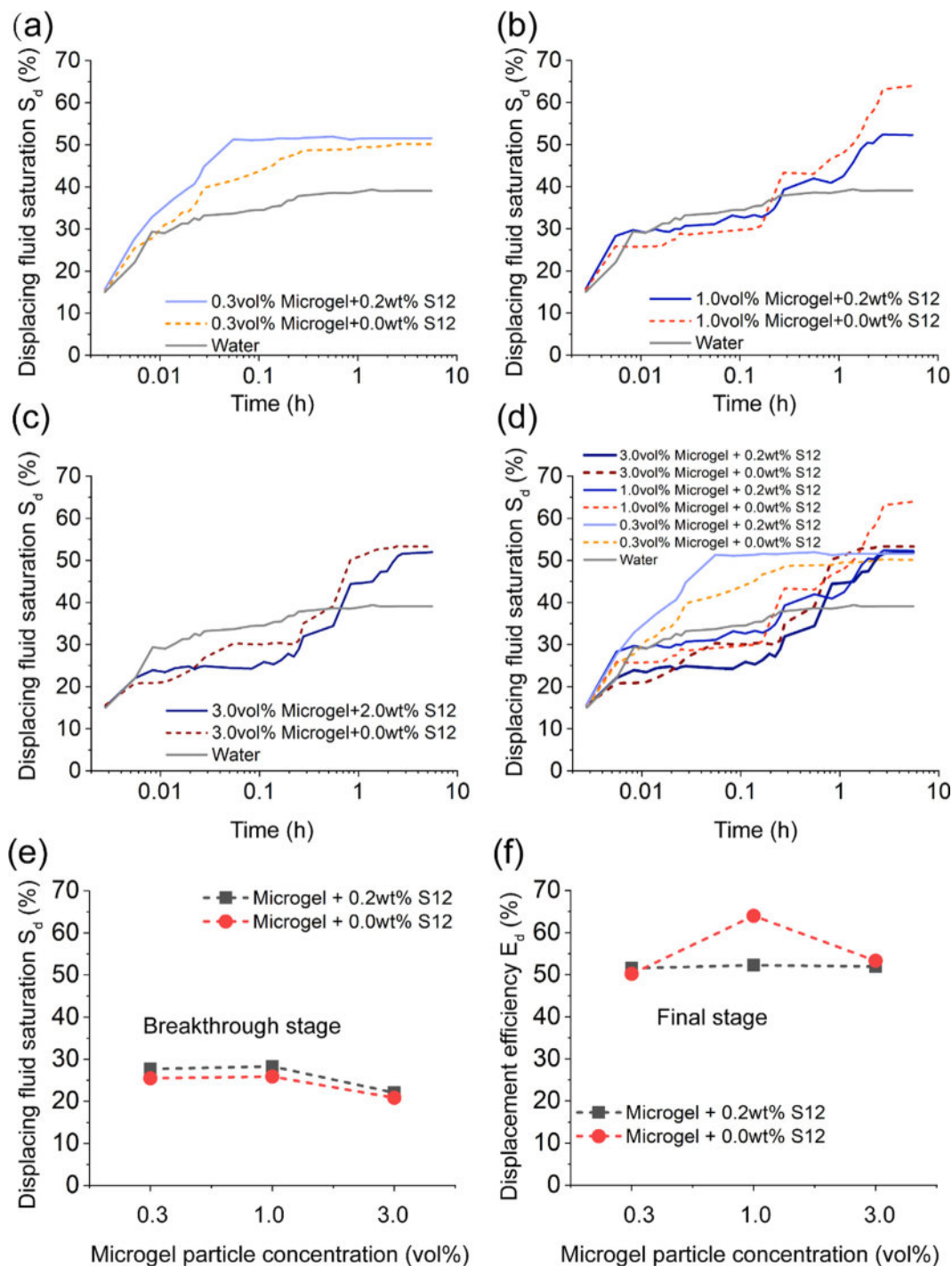


Fig. 6. Displacing fluid saturation or displacement efficiency curves of microgel particle suspensions in the absence and presence of surfactant-S12 at (a) low particle concentration 0.3 vol.%, (b) intermediate particle concentration 1.0 vol.%, and (c) high particle concentration 3.0 vol.%, where the saturation curve of waterflooding under the same condition was introduced for comparison. (d) The displacing fluid saturation curves of all floods. (e, f) The variations in displacing fluid saturation at (e) the breakthrough stage and displacement efficiency at (f) the final stage versus microgel particle concentrations in the absence and presence of surfactant-S12, where $E_d = S_d$ at the final stage.

tion of larger oil clusters (the five largest oil clusters were chosen in this paper), as shown in Fig. 7. Compared with the cases in the presence of surfactant-S12 (plain microgel particles), at the low particle concentration, suspensions in the absence of surfactant-S12 always obtain a lesser ganglion number and sweep the smaller matrix region (Fig. 7a,d); at the intermediate particle concentration, it can get the lesser ganglion number and smaller cluster volume, which means stronger sweeping and carrying abilities in the

matrix region (Fig. 7b,e); conversely, at the high concentration, it can get the moderate ganglion number and the smaller sweep area in the matrix region (Fig. 7c,f). To present the statistical oil ganglia configuration influenced by microgel particle suspension with and without surfactant-S12, we summarized the ganglia diameter distribution at the final stage, as shown in Fig. 7g-i. Small ganglia (Feret diameter less than 100um) produce the most ganglion number, while larger clusters occupy the largest volume fraction of

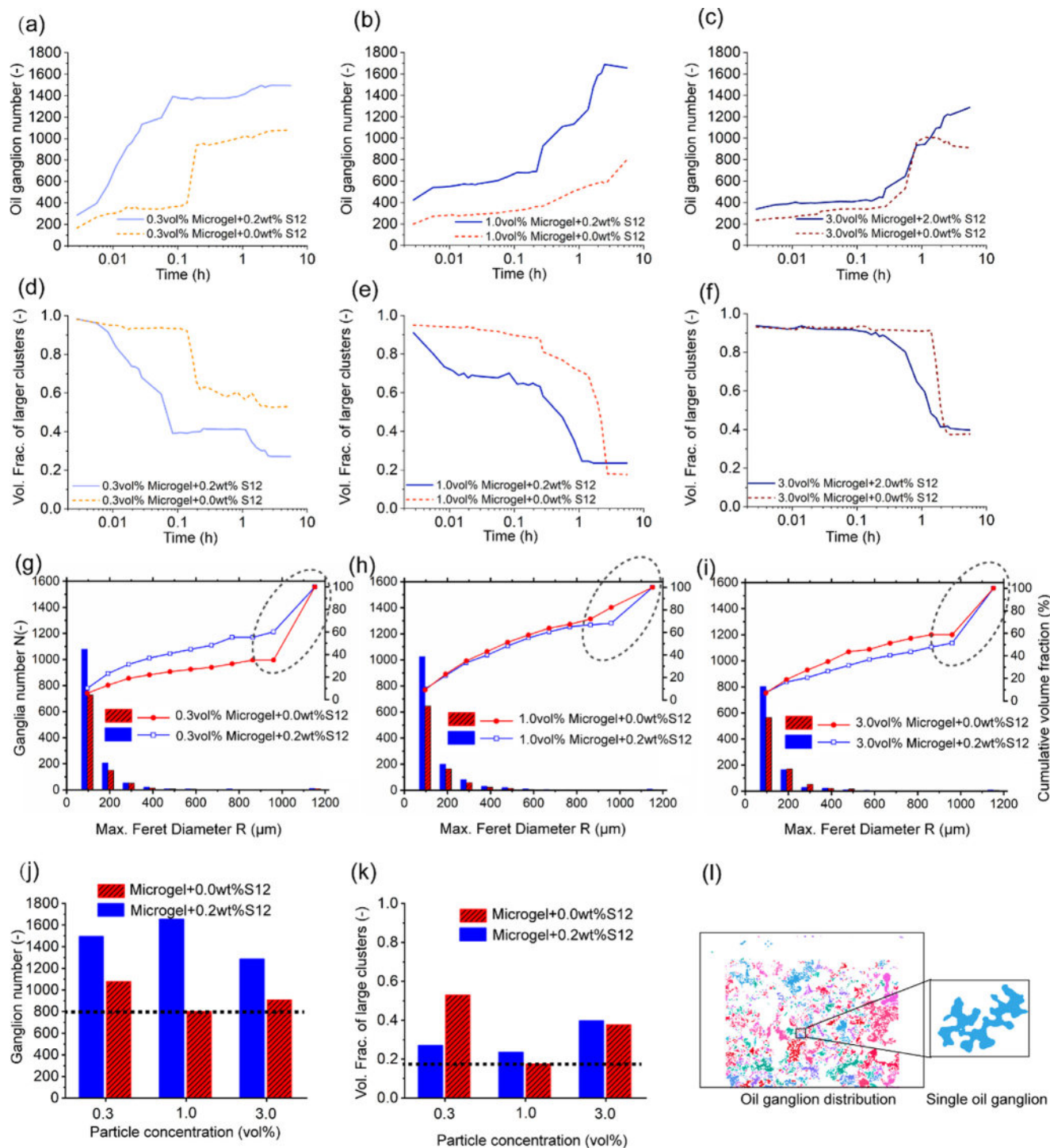


Fig. 7. The increase in oil ganglion number versus time at the microgel particle concentration of (a) 0.3 vol.%, (b) 1.0 vol.%, and (c) 3.0 vol.%. The decline in volume fraction of larger clusters at the microgel particle concentration of (d) 0.3 vol.%, (e) 1.0 vol.%, and (f) 3.0 vol.%. Ganglia diameter distribution and the cumulative volume fraction at the microgel particle concentration of (g) 0.3 vol.%, (h) 1.0 vol.%, and (i) 3.0 vol.%. The differences in (j) ganglion number and (k) volume fraction of larger clusters at the final stage of the suspension flooding. (l) Schematic diagram of oil ganglion distribution and the individual oil ganglia.

ganglia in porous media. When preferential flow occurs, a clear separation in ganglia size is evident in the cumulative volume fraction curve (Fig. 7g–i). Examining the distribution of ganglia volumes demonstrates that a single well-connected cluster is present, as are many disconnected ganglia with much smaller volumes. Microgel particle suspension at 1.0 vol.% in the absence of surfactant-S12 (with moderate content of microgel-in-oil) can

suppress preferential flow conditions and reconnect preferential flow pathways with the trapped ganglia in the matrix region (Fig. 7h).

Ganglion number and volume fraction of large clusters at the final stage indicate that suspensions with moderate microgel-in-oil can sweep the matrix region widely and remove the tiny oil droplets immediately to avoid oil droplets trapped in the porous

structure (Fig. 7j, k). Combining these results with the displacement performance (Fig. 5, Fig. 6), we can see that decreasing the contact angle and the interfacial tension slightly by adding surfactant-S12 does not significantly increase the displacement efficiency in such heterogeneous porous media. Although some oil clusters can be peeled off as isolated ganglia, the oil phase may not be carried out from the matrix due to the Jamin effect - oil droplets hindering the oil phase transport pathway. In contrast, microgel particle suspension with moderate content of microgel-in-oil can slowly increase the ganglion number and rapidly decrease the volume fraction of larger oil clusters at the late displacement stage, which may be an important manifestation that the oil peeled off from the large oil clusters in the matrix can be transported to the PFP region directly. The synergistic transport behavior of microgel-in-oil and plain microgel particles in the

PFP region is responsible for these topological characteristics, contributing to this high displacement efficiency.

3.5. Evolution of pressure difference

Unlike plain microgel particles passing the PFP region directly, the synergistic transport of microgel-in-oil and plain microgel particles in the PFP region present the retention-accumulation-release mode with the flow field fluctuation, as shown in Fig. 8. Based on the evolution of injection pressure (Fig. 8a), oil ganglion (Fig. 7), and displacement efficiency (Fig. 6), we can conclude that microgel-in-oil can continuously generate effective flow field fluctuations to drive large clusters out from the matrix region and achieve a higher displacement efficiency eventually. When several microgel-in-oil are stuck in the PFP region, the subsequent well-

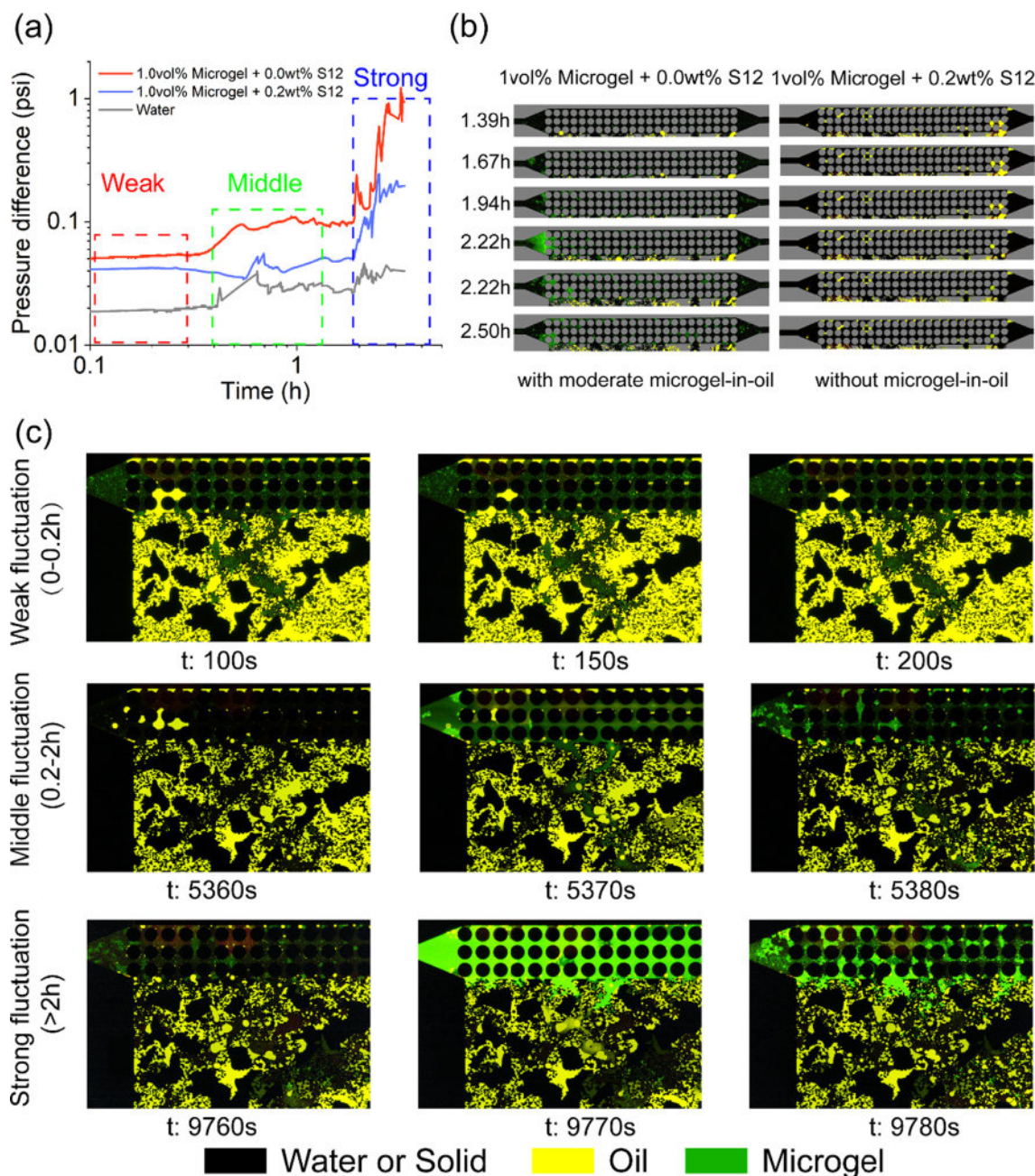


Fig. 8. Evolution of injection pressure and particle distribution in the preferential flow pathway. (a) Pressure difference curves during the displacement experiments. (b) Blockage and release in the PFP region caused by microgel-in-oil, compared with well-dispersed microgel particles using surfactant-S12. (c) Local view images of microgel-in-oil transport and retention in the PFP region during different displacement stages.

dispersed microgel particles will gradually accumulate in this area by the filtering effect. The pressure difference between the inlet and outlet will increase progressively until the local critical pressure value is reached. Then, these particles will be washed away, and the pressure difference will drop sharply as the preferential flow pathway is dredged. Fig. 8b presents the transport process of 1.0 vol% microgel particle suspension in the absence and presence of surfactant-S12. Even though the content of microgel-in-oil is ultralow compared with microgel particle content, microgel-in-oil still plays a crucial role in the retention-accumulation-release process. From the pressure difference curve in Fig. 8a, we can see that the fluctuation effect can be divided into three stages: weak fluctuation (0–0.2 h), moderate fluctuation (0.2–2 h), and strong fluctuation (>2 h). The corresponding microscopic images of the microgel particle transport process and its effect on improving displacement efficiency in the matrix area of the heterogeneous porous media are shown in Fig. 8c. The effect of microgel-in-oil is time-dependent due to the particle accumulation process in the PFP region, which leads to the fluctuation phenomena from the weak to the strong level and presents self-adaptive to the displacement process. In the early stage (0–0.2 h), few microgel-in-oil were retained in the PFP region, and the flow field fluctuation effect was weak. Then, in the middle stage (0.2–2 h), a small amount of microgel-in-oil appeared and formed a local flow field fluctuation, which caused the residual oil trapped in the matrix area near the PFP region to be swept carried out effectively. In the final stage (>2 h), many microgel-in-oil were stuck in PFP and caused rapid particle retention-accumulation-release phenomena, leading to strong flow field fluctuations. Since a large amount of residual oil in the matrix area nearby the PFP region has been carried out in the early and middle stages, this strong fluctuation of the flow field may contribute to displacing the residual oil from the deeper part of the matrix area.

The retention-accumulation-release mode can achieve the strong sweeping and carrying ability of displacing fluid in the deep matrix region. On the one hand, a higher injection pressure leads to a lower fraction of large clusters and a stronger sweeping ability. On the other hand, the carrying ability is determined by the competition between the pressure drop $|\Delta P_v| = \eta(Q/A)L_g/K$ and the capillary resistance induced by the fluid–fluid interface through the pores $|\Delta P_c| \approx \gamma/d$, where η is the displacing fluid viscosity, Q is the flow rate, A is the cross-sectional area, L_g is the ganglia length, K is the permeability, γ is the fluid–fluid interfacial tension, and d is the characteristic pore size. Weak-to-strong pressure fluctuation can increase pressure drop and slowly increase the ganglion number to suppress the capillary resistance increasing, thus increasing the carrying ability. Stronger sweeping and carrying abilities will contribute to the highest displacement efficiency.

However, it should be noted that these displacement mechanisms presented here are from an idealized suspension condition where the plain particle size is much smaller than the pore size of the PFP region, and the particle swelling may not change this condition because all microfluidic experiments are finished within 4 h. When the size of plain microgel particles is comparable to or larger than the pore size, the plugging effect of plain microgel particles cannot be ignored in porous media. Moreover, the statistical distribution of preferential flow pathways in the natural porous media may lead to more complex particle transport behavior, so modifications should be introduced for the optimal displacement conditions. All those problems should be analyzed in the future work.

4. Conclusions

In this study, microgel-in-oil as a high-performance displacement additive was proposed and realized to improve displacement

efficiency in heterogeneous porous media. The spontaneous formation of microgel-in-oil and their coexistence with plain microgel particles in the suspension were characterized based on fluorescence microscopy and Cryo-SEM observations. Although the transport behavior of plain microgel particles and their corresponding effect on displacement efficiency have been discussed in previous studies [8,31,62], microgel-in-oil as an equally important component in the suspension has not been reported yet, and the direct link to pore-scale characteristics of these particles to corresponding flow behavior in porous media remained missing.

Based on microfluidic chips with the heterogeneous porous structure containing the preferential flow pathway, the dependence of the multiphase displacement response on the particle transport behavior was assessed by the analysis of phase saturation, phase topology, and pressure field. By varying microgel particle concentration, displacement processes of microgel particle suspension with microgel-in-oil are identified: the direct passing mode at low particle concentration, the retention-accumulation-release mode at intermediate particle concentration, and the plugging mode at high particle concentration. Microgel particle suspension with moderate microgel-in-oil content can effectively displace the trapped displaced fluid from the matrix region without harming the main flow channel. They rapidly decrease the volume fraction of larger clusters but slowly increase the ganglion number simultaneously, leading to strong sweeping and carrying abilities to achieve the best displacement. Fewer microgel-in-oil cannot alter the flow direction, while too many microgel particles will block the PFP region directly. Based on injection pressure, oil ganglion, and fluid saturation evolution, we demonstrate that microgel-in-oil can continuously generate flow field fluctuations in the PFP region to drive larger oil clusters out from the deep matrix region. This pressure fluctuation is time-dependent due to the gradual retention of the microgel-in-oil in the preferential flow pathway.

Moving forward, for the engineering application of microgel-in-oil suspension, more essential factors should be considered, such as asphaltenes or surfactants in the displaced fluid [63], high salinity [64], and higher temperature/pressure [65] in the underground. Wettability also plays an important role in multiphase displacement in heterogeneous porous media [55,66]; coupling the wettability alteration effect and microgel-in-oil may promote better displacement consequences. Regardless, the current outcomes and novel design of microgel-in-oil pave the way for new strategies for effective suspension displacement in geological systems, such as enhanced oil recovery, soil remediation, and CO₂ sequestration.

CRediT authorship contribution statement

Wenhai Lei: Investigation, Validation, Writing – original draft. **Xukang Lu:** Investigation, Writing – original draft. **Tianjiang Wu:** Validation. **Haien Yang:** Writing – review & editing. **Moran Wang:** Conceptualization, Supervision, Writing – review & editing, Project administration.

Declaration of Competing Interest

The authors declare that they have no known competing financial interests or personal relationships that could have appeared to influence the work reported in this paper.

Acknowledgments

This work is financially supported by the NSF grant of China (No. U1837602, 91634107) and the National Key Research and Development Program of China (No. 2019YFA0708704). We would like to sincerely acknowledge Dr. Mengquan Shi from the Technical

Institute of Physics and Chemistry, Chinese Academy of Sciences, for his help with microgel particle synthesis.

References

- L.W. Lake, *Enhanced Oil Recovery*, Prentice Hall, Englewood Cliffs, 1989.
- T. Pak, L.F.d.L. Luz, T. Tosco, G.S.R. Costa, P.R.R. Rosa, N.L. Archilha, Pore-scale investigation of the use of reactive nanoparticles for in situ remediation of contaminated groundwater source, *Proc. Natl. Acad. Sci. U. S. A.* 117(24) (2020) 13366.
- H.E. Huppert, J.A. Neufeld, The fluid mechanics of carbon dioxide sequestration, *Annu. Rev. Fluid Mech.* 46 (1) (2014) 255–272.
- M. Huang, W. Lei, M. Wang, S. Zhao, C. Li, M. Wang, H. Zhu, Large area high-performance bismuth vanadate photoanode for efficient solar water splitting, *J. Mater. Chem. A* 8 (7) (2020) 3845–3850.
- N. Hao, Y. Nie, J.X.J. Zhang, Microfluidics for silica biomaterials synthesis: opportunities and challenges, *Biomater. Sci.* 7 (6) (2019) 2218–2240.
- Y. Ju, W. Gong, W. Chang, M. Sun, Effects of pore characteristics on water-oil two-phase displacement in non-homogeneous pore structures: a pore-scale lattice Boltzmann model considering various fluid density ratios, *Int. J. Eng. Sci.* 154 (2020) 103343.
- Y. Ju, W. Gong, J. Zheng, Characterization of immiscible phase displacement in heterogeneous pore structures: Parallel multicomponent lattice Boltzmann simulation and experimental validation using three-dimensional printing technology, *Int. J. Multiph. Flow* 114 (2019) 50–65.
- C. Xie, W. Lei, M.T. Balhoff, M. Wang, S. Chen, Self-adaptive preferential flow control using displacing fluid with dispersed polymers in heterogeneous porous media, *J. Fluid Mech.* 906 (2021) A10.
- H. Zhang, T.S. Ramakrishnan, A. Nikolov, D. Wasan, Enhanced oil displacement by nanofluid's structural disjoining pressure in model fractured porous media, *J. Colloid. Interface. Sci.* 511 (2018) 48–56.
- S.S. Datta, T.S. Ramakrishnan, D.A. Weitz, Mobilization of a trapped non-wetting fluid from a three-dimensional porous medium, *Phys. Fluids* 26 (2) (2014) 022002.
- Y. Khoshkalam, M. Khosravi, B. Rostami, Visual investigation of viscous cross-flow during foam injection in a matrix-fracture system, *Phys. Fluids* 31 (2) (2019) 023102.
- D.-K. Han, C.-Z. Yang, Z.-Q. Zhang, Z.-H. Lou, Y.-I. Chang, Recent development of enhanced oil recovery in China, *J. Pet. Sci. Eng.* 22 (1) (1999) 181–188.
- S. Parsa, E. Santanach-Carreras, L. Xiao, D.A. Weitz, Origin of anomalous polymer-induced fluid displacement in porous media, *Phys. Rev. Fluids* 5 (2) (2020) 022001.
- Y. Debbabi, M.D. Jackson, G.J. Hampson, P.J.R. Fitch, P. Salinas, Viscous crossflow in layered porous media, *Transp. Porous Media* 117 (2) (2017) 281–309.
- C. Xie, W. Lv, M. Wang, Shear-thinning or shear-thickening fluid for better EOR?—a direct pore-scale study, *J. Pet. Sci. Eng.* 161 (2017) 683–691.
- C.A. Browne, A. Shih, S.S. Datta, Pore-scale flow characterization of polymer solutions in microfluidic porous media, *Small* 16 (9) (2020) 1903944.
- H. Yang, S. Shao, T. Zhu, C. Chen, S. Liu, B. Zhou, X. Hou, Y. Zhang, W. Kang, Shear resistance performance of low elastic polymer microspheres used for conformance control treatment, *J. Ind. Eng. Chem.* 79 (2019) 295–306.
- M. Abdulbaki, C. Huh, K. Sepelhrnoori, M. Delshad, A. Varavei, A critical review on use of polymer microgels for conformance control purposes, *J. Pet. Sci. Eng.* 122 (2014) 741–753.
- G. Zhao, Q. You, J. Tao, C. Gu, H. Aziz, L. Ma, C. Dai, Preparation and application of a novel phenolic resin dispersed particle gel for in-depth profile control in low permeability reservoirs, *J. Pet. Sci. Eng.* 161 (2018) 703–714.
- A. Imqam, B. Bai, M. Delshad, Micro-particle gel transport performance through unconsolidated sandstone and its blocking to water flow during conformance control treatments, *Fuel* 231 (2018) 479–488.
- J. Li, Z. Jiang, Y. Wang, J. Zheng, G. Huang, Stability, seepage and displacement characteristics of heterogeneous branched-preformed particle gels for enhanced oil recovery, *RSC Adv.* 8 (9) (2018) 4881–4889.
- A.J.P. Fletcher, S. Flew, I.N. Forsdyke, J.C. Morgan, C. Rogers, D. Suttles, Deep diverting gels for very cost-effective waterflood control, *J. Pet. Sci. Eng.* 7 (1) (1992) 33–43.
- C.A. Grattoni, H.H. Al-Sharji, C. Yang, A.H. Muggeridge, R.W. Zimmerman, Rheology and permeability of crosslinked polyacrylamide gel, *J. Colloid. Interface. Sci.* 240 (2) (2001) 601–607.
- M. Bjørsvik, H. Høiland, A. Skauge, Formation of colloidal dispersion gels from aqueous polyacrylamide solutions, *Colloid Surf. A-Physicochem. Eng. Asp.* 317 (1) (2008) 504–511.
- J. Leng, M. Wei, B. Bai, Review of transport mechanisms and numerical simulation studies of preformed particle gel for conformance control, *J. Pet. Sci. Eng.* 206 (2021) 109051.
- B. Bai, H. Zhang, Preformed-particle-gel transport through open fractures and its effect on water flow, *SPE J.* 16 (02) (2011) 388–400.
- W. Lei, C. Xie, T. Wu, X. Wu, M. Wang, Transport mechanism of deformable micro-gel particle through micropores with mechanical properties characterized by AFM, *Sci. Rep.* 9 (1) (2019) 1453.
- C. Dai, Y. Liu, C. Zou, Q. You, S. Yang, M. Zhao, G. Zhao, Y. Wu, Y. Sun, Investigation on matching relationship between dispersed particle gel (DPG) and reservoir pore-throats for in-depth profile control, *Fuel* 207 (2017) 109–120.
- R. Ranganathan, R. Lewis, C.S. McCool, D.W. Green, G.P. Willhite, Experimental study of the gelation behavior of a polyacrylamide/aluminum citrate colloidal-dispersion gel system, *SPE J.* 3 (04) (1998) 337–343.
- C. Yao, G. Lei, L.M. Cathles, T.S. Steenhuis, Pore-scale investigation of micron-size polyacrylamide elastic microspheres (MPeMs) transport and retention in saturated porous media, *Environ. Sci. Technol.* 48 (9) (2014) 5329–5335.
- W. Lei, Q. Li, H.-E. Yang, T.-J. Wu, J. Wei, M. Wang, Preferential flow control in heterogeneous porous media by concentration-manipulated rheology of microgel particle suspension, *J. Pet. Sci. Eng.* 212 (2022) 110275.
- E. Dickinson, Structure and rheology of colloidal particle gels: Insight from computer simulation, *Adv. Colloid Interface Sci.* 199 (2013) 114–127.
- M. Lin, G. Zhang, Z. Hua, Q. Zhao, F. Sun, Conformation and plugging properties of crosslinked polymer microspheres for profile control, *Colloid Surf. A-Physicochem. Eng. Asp.* 477 (2015) 49–54.
- W. Lei, T. Liu, C. Xie, H. Yang, T. Wu, M. Wang, Enhanced oil recovery mechanism and recovery performance of micro-gel particle suspensions by microfluidic experiments, *Energy Sci. Eng.* 8 (4) (2020) 986–998.
- B. Bai, Y. Liu, J.-P. Coste, L. Li, Preformed particle gel for conformance control: transport mechanism through porous media, *SPE Reserv. Eval. Eng.* 10 (02) (2007) 176–184.
- S. Zhao, W. Pu, B. Wei, X. Xu, A comprehensive investigation of polymer microspheres (PMs) migration in porous media: EOR implication, *Fuel* 235 (2019) 249–258.
- H.A. Stone, A.D. Stroock, A. Ajdari, Engineering flows in small devices: microfluidics toward a lab-on-a-chip, *Annu. Rev. Fluid Mech.* 36 (1) (2004) 381–411.
- D. Sinton, Energy: the microfluidic frontier, *Lab Chip* 14 (17) (2014) 3127–3134.
- A. Anbari, H.T. Chien, S.S. Datta, W. Deng, D.A. Weitz, J. Fan, Microfluidic model porous media: fabrication and applications, *Small* 1703575 (2018).
- N.S. Kumar Gunda, B. Bera, N.K. Karadimitriou, S.K. Mitra, S.M. Hassanizadeh, Reservoir-on-a-Chip (ROC): a new paradigm in reservoir engineering, *Lab Chip* 11 (22) (2011) 3785–3792.
- C.E. Stanley, G. Grossmann, X. Casadevall i Solvas, A.J. deMello, Soil-on-a-Chip: microfluidic platforms for environmental organismal studies, *Lab Chip* 16(2) (2016) 228–241.
- L. Mejia, P. Zhu, J.D. Hyman, K.K. Mohanty, M.T. Balhoff, Coreflood on a chip: core-scale micromodels for subsurface applications, *Fuel* 281 (2020) 118716.
- T.W. de Haas, H. Fadaei, U. Guerrero, D. Sinton, Steam-on-a-chip for oil recovery: the role of alkaline additives in steam assisted gravity drainage, *Lab. Chip.* 13 (19) (2013) 3832–3839.
- C.L. Gao, J. Wegner, L. Ganzer, Real structure micromodels based on reservoir rocks for enhanced oil recovery (EOR) applications, *Lab. Chip.* 20 (12) (2020) 2197–2208.
- J. Wan, T.K. Tokunaga, C.-F. Tsang, G.S. Bodvarsson, Improved glass micromodel methods for studies of flow and transport in fractured porous media, *Water Resour. Res.* 32 (7) (1996) 1955–1964.
- K. Ma, R. Lontas, C.A. Conn, G.J. Hirasaki, S.L. Biswal, Visualization of improved sweep with foam in heterogeneous porous media using microfluidics, *Soft Matter* 8 (41) (2012) 10669.
- C.A. Conn, K. Ma, G.J. Hirasaki, S.L. Biswal, Visualizing oil displacement with foam in a microfluidic device with permeability contrast, *Lab Chip* 14 (20) (2014) 3968–3977.
- K. Xu, P. Zhu, T. Colon, C. Huh, M. Balhoff, A microfluidic investigation of the synergistic effect of nanoparticles and surfactants in macro-emulsion-based enhanced oil recovery, *SPE J.* 22 (02) (2017) 459–469.
- V. Lazouskaya, Y. Jin, D. Or, Interfacial interactions and colloid retention under steady flows in a capillary channel, *J. Colloid. Interface. Sci.* 303 (1) (2006) 171–184.
- O. Torres, B. Murray, A. Sarkar, Emulsion microgel particles: Novel encapsulation strategy for lipophilic molecules, *Trends Food Sci. Technol.* 55 (2016) 98–108.
- O. Torres, E. Andablo-Reyes, B.S. Murray, A. Sarkar, Emulsion microgel particles as high-performance bio-lubricants, *ACS Appl. Mater. Interfaces* 10 (32) (2018) 26893–26905.
- E. An, C.B. Jeong, C. Cha, D.H. Kim, H. Lee, H. Kong, J. Kim, J.W. Kim, Fabrication of microgel-in-liposome particles with improved water retention, *Langmuir* 28 (9) (2012) 4095–4101.
- C. Xie, W. Lei, M. Wang, Lattice boltzmann model for three-phase viscoelastic fluid flow, *Phys. Rev. E* 97 (2) (2018) 023312.
- C. Chomsurin, C.J. Werth, Analysis of pore-scale nonaqueous phase liquid dissolution in etched silicon pore networks, *Water Resour. Res.* 39 (9) (2003) 1265.
- W. Lei, X. Lu, F. Liu, M. Wang, Non-monotonic wettability effects on displacement in heterogeneous porous media, *J. Fluid Mech.* 942 (2022) R5.
- N.R. Morrow, I. Chatzis, J.J. Taber, Entrapment and mobilization of residual oil in bead packs, *SPE Reserv. Eng.* 3 (03) (1988) 927–934.
- H. Monteillet, M. Workamp, J. Appel, J.M. Kleijn, F.A.M. Leermakers, J. Sprakel, Ultrastrong anchoring yet barrier-free adsorption of composite microgels at liquid interfaces, *Adv. Mater. Interfaces* 1 (7) (2014) 1300121.
- R.W. Style, L. Isa, E.R. Dufresne, Adsorption of soft particles at fluid interfaces, *Soft Matter* 11 (37) (2015) 7412–7419.
- Y. Gong, Z. Zhang, J. He, Deformation and stability of core-shell microgels at oil/water interface, *Ind. Eng. Chem. Res.* 56 (50) (2017) 14793–14798.
- R.A. Gumerov, A.M. Romyantsev, A.A. Rudov, A. Pich, W. Richtering, M. Möller, I.I. Potemkin, Mixing of two immiscible liquids within the polymer microgel adsorbed at their interface, *ACS Macro Lett.* 5 (5) (2016) 612–616.

- [61] M.V. Anakhov, R.A. Gumerov, W. Richtering, A. Pich, I.I. Potemkin, Scavenging one of the liquids versus emulsion stabilization by microgels in a mixture of two immiscible liquids, *ACS Macro Lett.* 9 (5) (2020) 736–742.
- [62] H. Zhao, M. Lin, Z. Dong, M. Li, G. Zhang, J. Yang, Study of deep profile control and oil displacement technologies with nanoscale polymer microspheres, *J. Colloid. Interface. Sci.* 424 (424) (2014) 67–74.
- [63] P. Mohammadinejad, N. Hosseinpour, N. Rahmati, M.R. Rasaei, Formation damage during oil displacement by aqueous SiO₂ nanofluids in water-wet/oil-wet glass micromodel porous media, *J. Pet. Sci. Eng.* 182 (2019) 106297.
- [64] Z. Li, T. Zhao, W. Lv, B. Ma, Q. Hu, X. Ma, Z. Luo, M. Zhang, Z.-Z. Yu, D. Yang, Nanoscale polyacrylamide copolymer/silica hydrogel microspheres with high compressive strength and satisfactory dispersion stability for efficient profile control and plugging, *Ind. Eng. Chem. Res.* 60 (28) (2021) 10193–10202.
- [65] J. Zheng, W. Lei, Y. Ju, M. Wang, Investigation of Spontaneous Imbibition Behavior in a 3D Pore Space Under Reservoir Condition by Lattice Boltzmann Method, *J. Geophys. Res.-Solid Earth* 126(6) (2021) e2021JB021987.
- [66] B. Zhao, C.W. MacMinn, R. Juanes, Wettability control on multiphase flow in patterned microfluidics, *Proc. Natl. Acad. Sci. U. S. A.* 113 (37) (2016) 10251–10256.